doi:10.4149/neo_2022_211016N1474

Dictamnine inhibits pancreatic cancer cell growth and epithelial-mesenchymal transition by blocking the PI3K/AKT signaling pathway

Zhi-Qiang ZHANG[1], Wen-Liang XUAN[1], Yang HUANG[1], Shuo REN[2], Tu-Ya WULAN[1], Ye SONG[1], Dong-Bo XUE[1], Wei-Hui ZHANG[1,*]

[1]*Department of General Surgery, The First Affiliated Hospital of Harbin Medical University, Harbin, China;* [2]*Department of Gastrointestinal Surgery, Sichuan Provincial Cancer Hospital, Chengdu, China*

**Correspondence: zhangweihui626@hotmail.com*

Received October 16, 2021 / Accepted February 21, 2022

Many different treatments are available for pancreatic cancer (PC), including surgical resection, chemotherapy, radiotherapy, and immunotherapy, but these treatments are often ineffective at curing PC. Hence, identifying new and effective agents or strategies to improve therapeutic effects is critical. This study focused on the efficacy of dictamnine (DTM), a furan quinoline alkaloid extracted from *Dictamnus dasycarpus Turcz.*, in treating PC. Our *in vitro* results showed that DTM can mitigate cell proliferation and induce cell cycle arrest and apoptosis in two different human PC cell lines. Moreover, epithelial-mesenchymal transition (EMT) was prevented during DTM treatment, reflected by reduced cell migration and invasion abilities. *In vivo* studies demonstrated that DTM treatment led to a remarkable inhibition of tumor growth in a xenograft nude mouse model. Mechanistic investigation showed that DTM might act by restraining constitutive and induced PI3K/AKT activity. In summary, our results demonstrated that DTM slows PC progression by inhibiting the activity of the PI3K/AKT signaling pathway and its downstream effectors and that DTM is effective as a pathway-specific cancer therapy. These findings could provide a greater understanding of the function of anticancer drugs and new options for PC treatment.

Key words: dictamnine; pancreatic cancer; apoptosis; cell cycle arrest; epithelial-mesenchymal transition; PI3K/AKT signaling

Pancreatic cancer (PC) is a highly fatal malignancy in humans and has been a major health concern since the beginning of this century [1]. Although multimodal treatment options are available for PC, it has a very unfavorable prognosis, with a low five-year survival of approximately 6% (ranging from 2% to 9%) [2]. Surgery remains the most effective method to treat PC, especially when diagnosed at an early stage; unfortunately, the majority of PC cases exhibit regional or distant metastases at the time of diagnosis, and surgical options are often limited [3]. In addition, PC has relatively low sensitivity to chemoradiotherapy, aggressive biological behaviors, and is unresponsive to available treatments, all resulting in therapeutic dilemmas [4]. Therefore, novel treatment strategies and drugs are urgently needed to effectively treat this malignant disease.

Certain drugs used in traditional Chinese medicine have shown good antitumor activity against malignant tumors with minor side effects. Dictamnine (DTM) is a component of the traditional herb *Dictamnus dasycarpus Turcz.*, and modern pharmacological studies have shown that it is effective against many pathological processes, such as slowing viral replication, inhibiting bacterial infection, and suppressing inflammatory responses [5–7]. A recent study by Wang *et al.* found that DTM has a significant inhibitory effect against several cancer types, such as colorectal and liver cancer [8]; however, the mechanism by which DTM inhibits PC development has not been revealed, which provides the motivation for our follow-up work.

Epithelial-mesenchymal transformation (EMT) is a crucial process that enables tumor development and is characterized by decreased expression of epithelial markers and increased expression of mesenchymal markers. Due to decreased intercellular adhesion and degradation of basement membranes via the EMT process, tumor cells can acquire motility and invasion abilities, which are essential for tumor growth and metastasis [9, 10]. As a highly aggressive malignancy, EMT induction has also been regarded as the main cause of PC cell migration, invasion, and metastasis [11, 12]. According to previous studies, reducing p-protein kinase B (p-AKT) levels in the phosphatidylinositol-3 kinase (PI3K)/AKT signaling pathway can weaken the EMT process in PC, suggesting that inhibition of the PI3K/AKT pathway contributes to reducing the ability of PC to metastasize [13, 14].

PI3K transduces intracellular signals and regulates various cellular processes involving lipid kinases; AKT is an important downstream effector of PI3K-mediated signal transduction. PI3K increases phosphatidylinositol-3,4,5-triphosphate (PIP3) formation, which promotes translocation of AKT to the cell membrane, where it is subsequently phosphorylated at Thr308 or Ser473 [15, 16]. Many researchers have demonstrated that the PI3K/AKT signaling is necessary for many aspects of tumor development, such as cell transformation, proliferation, growth, motility, and survival [17]. Approximately half of the patients with PC exhibit a corresponding increase in the PI3K/AKT signaling. Upregulation of the PI3K/AKT signaling pathway may lead to an unfavorable prognosis and low-grade tumor differentiation, whereas inhibiting this pathway blocks cell cycle progression and induces apoptosis in PC cells [13, 18]. These findings provide a theoretical basis and research direction for further study of targeted tumor therapy.

Our study results indicate that DTM reduces the levels of phosphorylated PI3K/AKT, thereby affecting a series of downstream proteins and, consequently, the malignant behavior of PC. In a murine xenograft model, DTM was effective at mitigating tumor growth. Moreover, no apparent hepatic or renal toxicity was observed in animals administered DTM. These results indicate that DTM may be a potential targeted therapeutic drug for human PC.

Materials and methods

Materials. DTM (HPLC ≥98%) was purchased from Shanghai Yuanye Bio-Technology Co., Ltd. (Shanghai, China). The primary antibodies (Abs) used in this research recognized the following proteins: PI3K (ab86714, Abcam), p-PI3K (Tyr458) (ab278545, Abcam), AKT (10176-2-AP, Proteintech), p-AKT (Ser473) (66444-1-Ig, Proteintech), Ki-67 (ab15580, Abcam), E-cadherin (#14472, CST), β-catenin (#8480, CST), vimentin (#5741, CST), cyclin D1 (#2922, CST), CDK6 (19117-1-AP, Proteintech), P21 (10355-1-AP, Proteintech), P27 (25614-1-AP, Proteintech), Bcl-2 (ab32124, Abcam), Bax (ab32503, Abcam), PARP/cleaved PARP (#9532, CST), and β-actin (ab8226, Abcam). The secondary Abs used in the study were obtained from Proteintech (Rosemont, IL, USA).

Cell culture. Human PC cell lines (PANC-1 and BxPC-3) and a human pancreatic duct epithelial cell line (hTERT-HPNE) were obtained from Shanghai Fuheng Biotechnology Co., Ltd. (Shanghai, China). The above cell lines were cultured in RPMI 1640 medium (HyClone China Ltd., China) supplemented with 10% fetal bovine serum (FBS; Gibco, Carlsbad, CA, USA) at 37 °C with 5% CO_2 and routinely passaged every 3 days. Each of the experiments described below was repeated three times.

Cell proliferation assay. Cell viability was determined with CCK-8 assays. Cells (5×10^3 cells/well) were plated in a medium (200 μl) in 96-well plates. After 24 h, the medium was replaced with a fresh complete medium containing specific concentrations of DTM (0–100 μM), and the cells were further incubated for different periods (0–24 h). At the indicated time points, CCK-8 solution was added to the wells for 90 min at 37 °C. Cell viability was determined with a microplate reader and is reported as the OD value at a wavelength of 490 nm.

Plate clonogenicity assay. Briefly, cells (1×10^3 cells/well) were seeded in 6-well plates and maintained overnight. The cells were then treated with DTM (0–80 μM) for another 24 h, after which the medium was replaced with a fresh culture medium containing 10% FBS, and the cells were cultured at 37 °C with 5% CO_2 for 14 days. Cell colonies were then fixed with methanol, stained with 0.5% crystal violet, and counted manually.

Tumor cell migration and invasion assays. A wound-healing assay was performed to evaluate cell migration. Cells were cultured in 6-well plates until they were completely confluent and then treated with DTM (60 μM) for 24 h. A scratch was then made in the cell monolayer with a plastic pipette tip (100 μl), and the cells were washed and maintained in a serum-free medium. The scratch width was recorded under a microscope (Olympus Corporation, Tokyo, Japan, 100× magnification) at 0 h and 24 h after scratching. Cell migration was quantified in multiple regions and is presented as the rate of closure.

Cell invasion was evaluated using a Transwell invasion assay. Matrigel and serum-free medium were added to the membrane in the upper Transwell chamber, which was air-dried for 2 h at 37 °C. A total of 5×10^3 cells in a serum-free medium (300 μl) were placed in the upper chambers, and the lower chambers were filled with a medium containing 10% FBS (500 μl). The cells were treated with DTM (60 μM) and incubated for 24 h, after which the cells on the membranes were stained with 0.5% crystal violet and analyzed under a microscope (Olympus, 400× magnification). The invasion ability of PC cells was quantified as the mean number of cells in three randomly selected fields.

Cell cycle analysis. Cells (approximately 1×10^6) were treated with DTM (60 μM) for 24 h before collection, stored in cold ethanol overnight, washed with PBS, and centrifuged (3000×g, 5 min). Afterward, 2.5 g/l RNase A and 40 μg/ml PI were added and incubated with the cell suspensions for 0.5 h in the dark. The cell cycle distribution was assessed via flow cytometry (BD Biosciences, Bedford, MA, USA).

Hoechst staining. Before cells were stained with Hoechst 33342 (Beyotime Institute of Biotechnology, Beijing, China), they were treated with DTM (60 μM) for 24 h. Apoptotic cells were identified under a fluorescence microscope (Olympus) based on morphological changes [19].

Apoptosis assay. Briefly, cells (3×10^3 cells/well) were plated in 6-well plates, cultured overnight, and then incubated with increasing doses of DTM (control, 20, 40, 60, or 80 μM) for 24 h or a fixed dose of DTM (60 μM) for 0, 4, 8, 16, or 24 h. Afterward, the cells were stained using reagents from

an Annexin V-FITC/PI Apoptosis Detection Kit (Thermo Fisher Scientific, MA, USA). Apoptotic cells were detected via flow cytometry (BD Biosciences). Morphological changes were also recorded under an inverted fluorescence microscope (Olympus).

Western blot analysis. Total protein was extracted from cells and tissues using RIPA buffer (Beyotime), mixed well, and homogenized several times. The protein concentrations were measured with a Bradford Protein Assay Kit (Beyotime). Equal amounts of protein (20–30 μg) were separated in 8–15% SDS-PAGE gels and then transferred onto PVDF membranes via electroblotting, after which the membranes were blocked with a 5% blocking solution. The membranes were then incubated with different primary Abs and corresponding HRP-labelled secondary Abs. The signals were assessed with an Odyssey infrared imaging system (LI-COR, Inc., Lincoln, NE, USA) according to the instrument instructions.

Immunofluorescence (IF) staining. For immunofluorescence assays, cells in confocal dishes were exposed to DTM (60 μM) for 24 h, fixed with 4% paraformaldehyde, and incubated with 0.3% Triton X-100 for 15 min. Primary Ab against p-AKT was added and incubated with the samples overnight at 4 °C. After the slides were repeatedly washed with PBS, a fluorescein isothiocyanate (FITC)-conjugated secondary Ab (CST, Danvers, MA, USA) was incubated with the slides for 1 h at 20 °C. Cell nuclei were stained with DAPI, and the slides were subjected to three additional 5 min washes before being sealed with an antifade reagent. Finally, the IF signals were observed via fluorescence microscopy (Olympus).

Molecular docking. The crystal structures of PI3K (PDB ID: 5JHB) [20] and AKT (PDB ID: 6S9W) [21] were obtained from RCSB PDB (https://www.rcsb.org/). The 3D structure of DTM (ZINC 265517 (dictamnine)) [8] was acquired from the Zinc database (https://zinc.docking.org/). A molecular docking test was performed to investigate the binding mode between the small molecule compound and the target proteins using AutoDock Vina 4.2. The molecular docking results were analyzed using PyMoL 2.3.4 software (http://www.pymol.org/).

Establishment of tumor xenografts in nude mice. Male BALB/c nude mice (5–6 weeks old, 19.1 ± 1.7 g) were obtained from VitalRiver Laboratory Animal Technology Co., Ltd. (Beijing, China). All experiments related to animals were approved by the Ethics Committee of the First Affiliated Hospital of Harbin Medical University on October 10, 2020 (No. 2, 020, 097). BxPC-3 cells (1×10^6) in PBS (10 μl) were injected into the right flanks of each mouse. One week later, BxPC-3 tumor-bearing nude mice (tumor volume approximately 100 mm^3) were randomly assigned to two groups (n=5): a DTM treatment group or a control group, which were intraperitoneally injected with DTM (15 mg/kg) or PBS, respectively, once a day. The tumor volume was calculated as $V = \text{length} \times \text{width}^2/2$. The experiment was terminated four weeks later, the nude mice were sacrificed, and the tumors were excised and photographed. Tumor tissues were processed for protein expression analysis and immunohistochemical staining. Liver and kidney tissues were stored in 4% paraformaldehyde at 4 °C for subsequent hematoxylin-eosin (H&E) staining and analysis.

Immunohistochemistry (IHC). Tumors were fixed with 4% paraformaldehyde, embedded in paraffin, and cut into 4 μm slices. Subsequently, the slices were incubated with Abs against target proteins. IHC staining was conducted using a diaminobenzidine substrate kit (Sigma). Images were captured under a vertical fluorescence microscope (Olympus).

ELISAs. To determine whether DTM damaged the visceral organs of nude mice, we used ELISA kits (Thermo) to assess the levels of alanine aminotransferase (ALT), aspartate aminotransferase (AST), and creatinine (Cr).

Statistical analysis. Quantitative data are expressed as the means ± standard deviation (SD). Differences between the two groups were analyzed by Student's t-test, and comparisons among multiple groups were conducted by one-way ANOVA. The data were statistically analyzed and visualized with GraphPad Prism software (GraphPad Software, La Jolla, CA, USA). p-values indicating statistically significant differences are presented with asterisks in the figures as follows: $^*p<0.05$ and $^{**}p<0.01$.

Results

DTM suppresses PC cell proliferation. DTM is a monomeric compound with a molecular weight of 199.21 Da, and the molecular structure of DTM is presented in Figures 1A and 1B. Recent pharmacological evaluations have revealed that some small molecules display significant cytotoxicity to cancer cells, and we decided to determine the effect of DTM on the viability of two PC cell lines (PANC-1 and BxPC-3) and human pancreatic duct epithelial cells (hTERT-HPNE) using a CCK-8 assay. By incubating PANC-1 and BxPC-3 cells with different concentrations of DTM (0–500 μM) for 24 h, we found that DTM noticeably reduced the proliferation of the two PC cell lines, with observed IC50 values of 66.35 and 58.55 μM, respectively; however, in the hTERT-HPNE cell line, this value was as high as 475.86 μM (Figure 1C). These results preliminarily indicated an inhibitory effect of DTM on PC cells, but no significant inhibition of normal human pancreatic duct cells was observed. In other words, DTM is specifically cytotoxic to PC cells.

DTM suppresses PC cell growth in a concentration- and time-dependent manner. To further explore the mode of action of DTM, we conducted the following tests. First, PANC-1, BxPC-3, and hTERT-HPNE cells were treated with various concentrations of DTM (0–100 μM) for 8, 16, and 24 h to evaluate the viability of the three cell lines (Figures 2A–2C). Then, a similar experiment was performed by exposing cells to a specific DTM concentration (60 μM) for

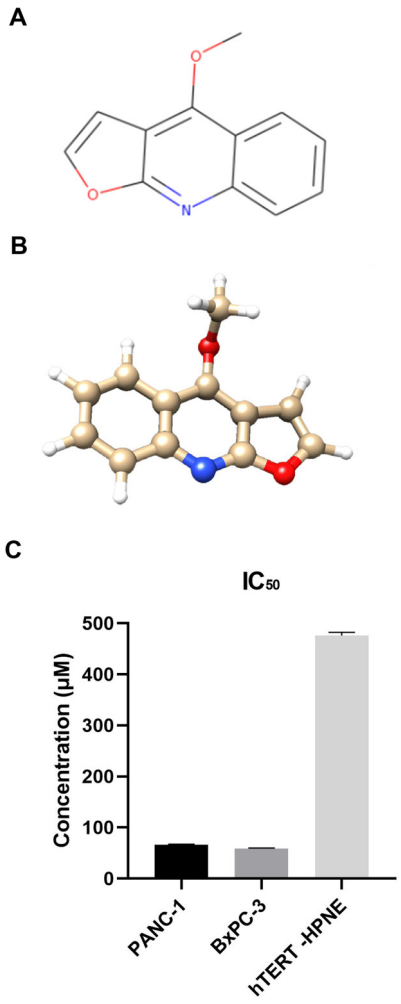

Figure 1. DTM suppresses PC cell proliferation. A) Chemical structure of DTM. B) 3D structure of DTM; the molecular formula is C12H9NO2. C) IC50 values for DTM in PANC-1, BxPC-3, and hTERT-HPNE cells. Different cells were treated with DTM (0–500 μM, 24 h), and cell viability was detected using CCK-8 assays. Abbreviations: DTM-dictamnine

multiple time periods (8, 16, and 24 h) (Figure 2D). The test results indicated that DTM significantly prevented the proliferation of PC cells but did not inhibit the growth of normal human pancreatic duct cells. We also found that the inhibitory effect became more obvious with increasing concentration and time. Subsequently, a clonogenic assay was performed to further investigate the effects of DTM on PC cells and hTERT-HPNE cell proliferation (Figure 2E). The experimental results showed that the colony-forming ability of PC cells decreased with increasing concentrations of DTM, but that of hTERT-HPNE cells was not affected by DTM (Figure 2F). According to the experimental data, we concluded that DTM not only reduces the viability of PC cells but also exhibits a concentration- and time-dependent effect.

DTM suppresses PC cell migration and invasion. As a manifestation of the metastatic ability of PC, we next investigated the ability of DTM to prevent PC cell migration and invasion. In wound healing assays (Figure 3A), we noted that the wound area observed between the cells 24 h after scratching was larger in cultures treated with DTM (60 μM) than in control cultures (Figure 3B). According to the results of Transwell assays (Figure 3C), the number of invading cells was diminished to a great extent after treatment with DTM (Figure 3D). In addition, the expression levels of EMT markers related to cell migration and invasion were determined. As shown in the western blotting analysis (Figures 3E, 3G), the expression levels of the mesenchymal markers vimentin and β-catenin were significantly reduced in PANC-1 and BxPC-3 cells treated with DTM, but the level of E-cadherin, an epithelial marker, was increased. As shown in Figures 3F and 3H, these changes exhibited dose- and time-dependent trends. These results indicate that PC cell migration and invasion were restrained by DTM through regulation of EMT-related marker levels.

DTM alters the expression of cell cycle-related proteins and induces G0/G1 phase arrest in PC cells. Flow cytometry was used to evaluate the effect of DTM on PC cell cycle progression (Figure 4A). After culture with DTM (60 μM, 24 h), increases were observed in the number of PANC-1 and BxPC-3 cells in the G0/G1 phase from 48.83% (control) to 59.79% and from 48.13% (control) to 60.81% (Figure 4B), respectively. Western blotting results revealed reduced cyclin D1 and CDK6 protein expression; however, the expression levels of P21 and P27, which are members of the Cip/Kip family that inhibit several cyclin-dependent kinase complexes (CDKs), were exceptionally high (Figures 4C, 4E). Furthermore, the expression of these key regulators related to G0/G1 transition was altered in a concentration- and time-dependent manner after DTM treatment (Figures 4D, 4F). These results suggest that DTM-induced G0/G1 phase arrest is one of the mechanisms by which PC cell proliferation is inhibited.

DTM induces PC cell apoptosis. The nuclear morphology of PC cells treated with DTM (60 μM) for 24 h was examined via staining with Hoechst 33342 to confirm a relationship between the DTM-mediated inhibition of cell proliferation and increased activation of the apoptotic pathway. Treated PC cells showed shrinkage, nuclear fragmentation or condensation, a reduction in cell volume, and other abnormal morphological characteristics (Figure 5A). The percentage of apoptotic cells is shown in Figure 5B. As shown in Figures 5C–5F and Supplementary Figures S1–S4, DTM treatment induced significant concentration- and time-dependent increases in the number of apoptotic PC cells. In addition, the expression of key proteins related to apoptosis was examined using western blotting (Figures 5G, 5I). The levels of Bcl-2 (an anti-apoptotic marker) and PARP were decreased and the levels of Bax (a proapoptotic marker) and cleaved PARP were increased in PC cells treated with

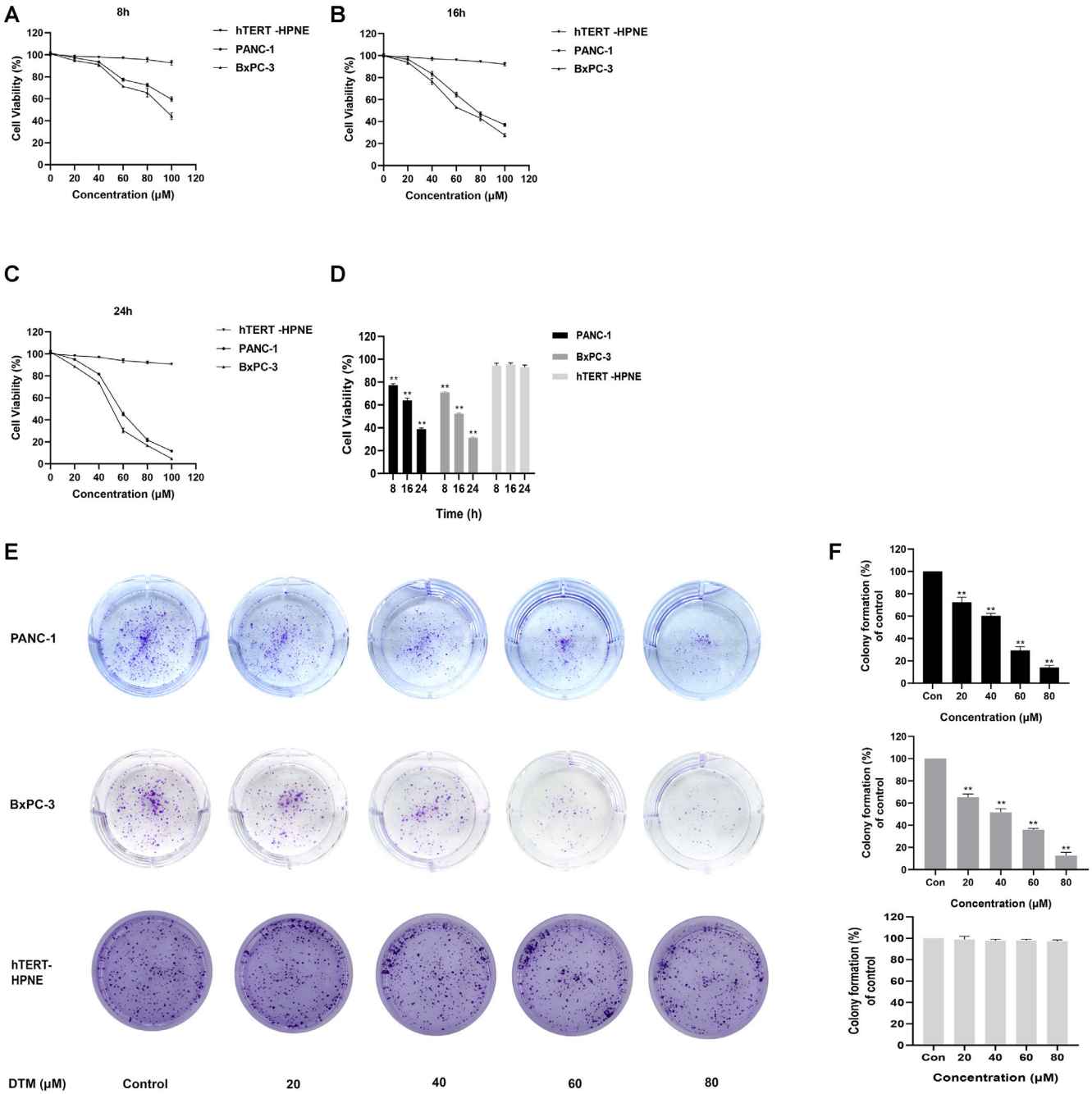

Figure 2. DTM suppresses PC cell growth in a concentration- and time-dependent manner. PANC-1, BxPC-3, and hTERT-HPNE cells were treated with 0–100 μM DTM for 8 h (A), 16 h (B), and 24 h (C), and the cell survival rate was determined using CCK-8 assays. D) Treatment with 60 μM DTM reduced the viability of PC cells in a time-dependent manner (8, 16, and 24 h). E) After treatment with DTM (0–80 μM), the colony formation ability of the two PC cell lines decreased but that of hTERT-HPNE cells was not affected by DTM. F) Comparison of the clone numbers of the two PC cell and hTERT-HPNE cell lines in each group. Notes: The analysis results are presented as the means ± standard deviations (n=3); *p<0.05, compared with the control group; **p<0.01, compared with the control group. Abbreviations: DTM-dictamnine; PC-pancreatic cancer

DTM (Figures 5H, 5J). Based on these results, DTM induces apoptosis by regulating the expression of apoptosis-related proteins, and this is one of the mechanisms through which DTM can inhibit the proliferation of PC cells.

DTM inhibits PI3K/AKT phosphorylation and prevents nuclear translocation of p-AKT. Numerous studies have shown that the PI3K/AKT pathway is a notable signaling target for the treatment of certain solid neoplasms

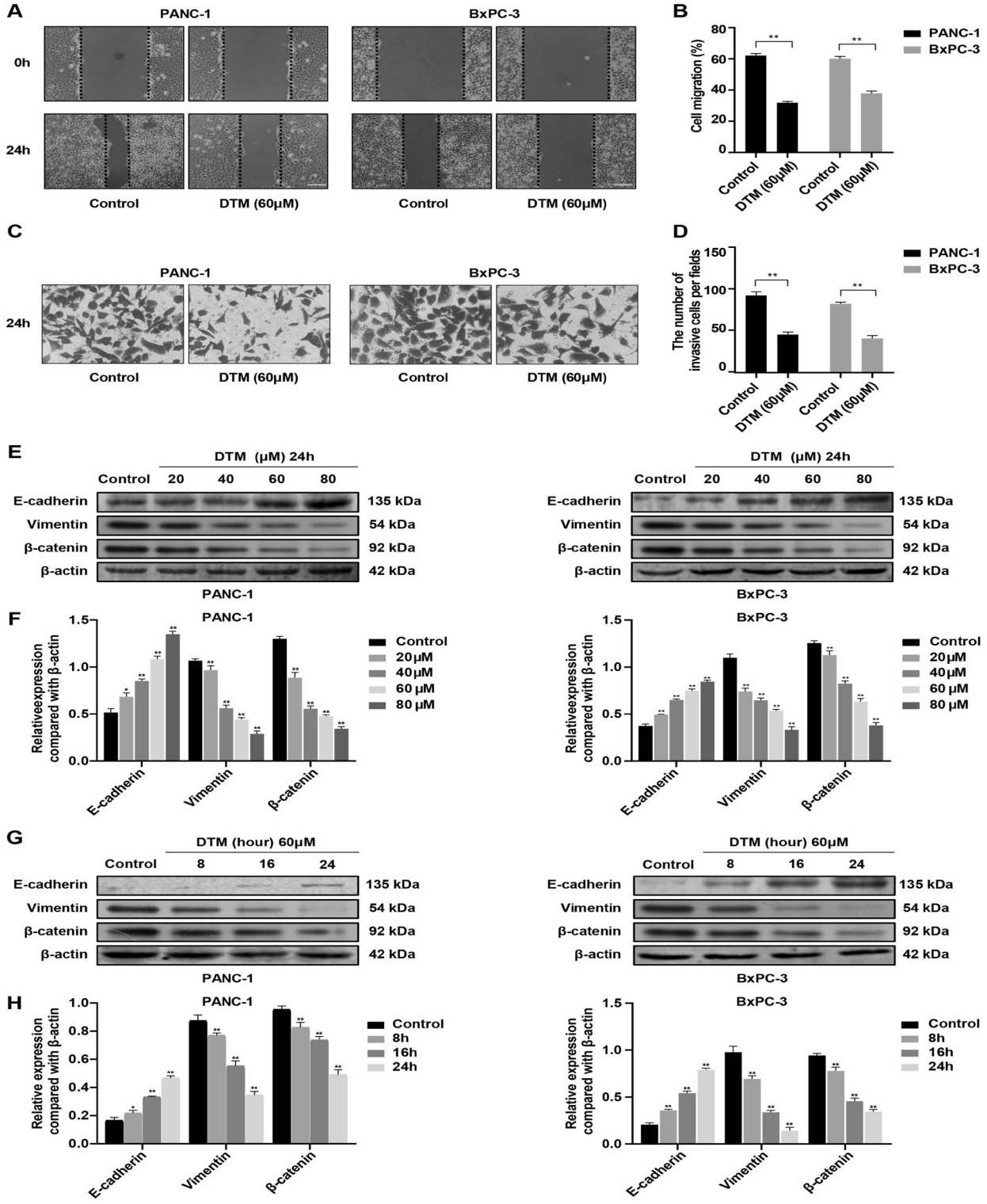

Figure 3. DTM suppresses PC cell migration and invasion. A) Wound healing assay of the two PC cell lines treated with DTM (60 μM, 24 h). Scale bar = 200 μm. B) Bar graphs represent migration rates. C) Transwell invasion assay of the two PC cell lines treated with DTM (60 μM, 24 h). Scale bar = 50 μm. D) Bar graphs represent invading cells. E, G) Western blots showing concentration- and time-dependent changes in the levels of EMT-related proteins in DTM-treated PC cells. F, H) Bar graphs represent the relative protein levels. Notes: The analysis results are presented as the means ± standard deviations (n=3); *p<0.05, compared with the control group; **p<0.01, compared with the control group. Abbreviations: DTM-dictamnine; PC-pancreatic cancer; PI3K-phosphatidylinositol-3 kinase; AKT-protein kinase B; EMT-epithelial-mesenchymal transition; E-cad-E-cadherin; β-cat-β-catenin; Vimen-vimentin

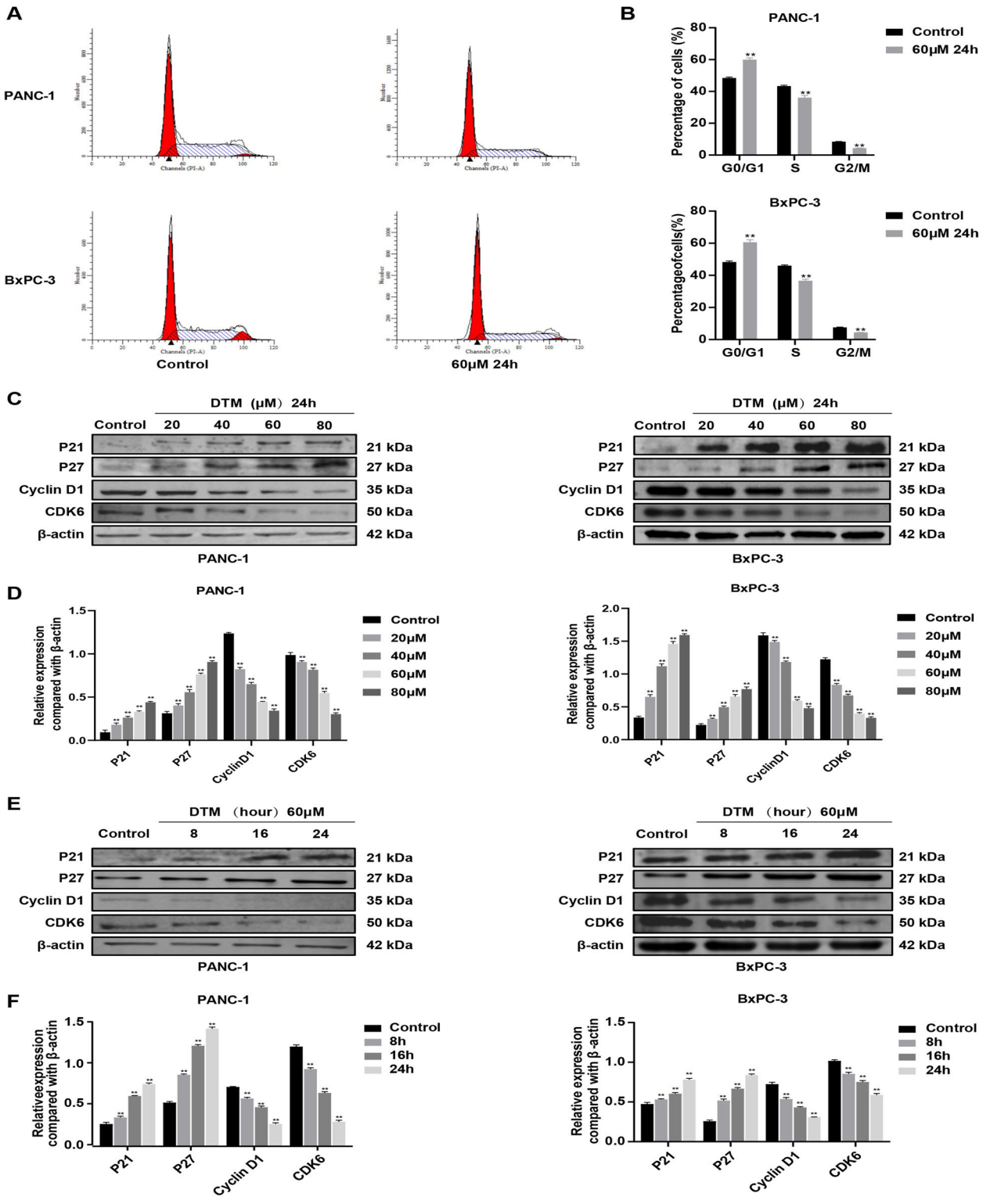

Figure 4. DTM alters the expression of cell cycle-related proteins and induces cell cycle arrest at the G0/G1 phase in PC cells. A) The cell cycle distributions of the two PC cell lines treated with DTM (60 μM, 24 h) were examined using flow cytometry. B) Quantification of the cell cycle distribution of the two PC cell lines. C, E) Densitometric analysis of the expression of cycle-related proteins in PC cells. D) Bar graphs represent relative protein expression. Notes: The analysis results are presented as the means ± standard deviations (n=3); *p<0.05, compared with the control group; **p<0.01, compared with the control group. Abbreviations: DTM-dictamnine; PC-pancreatic cancer

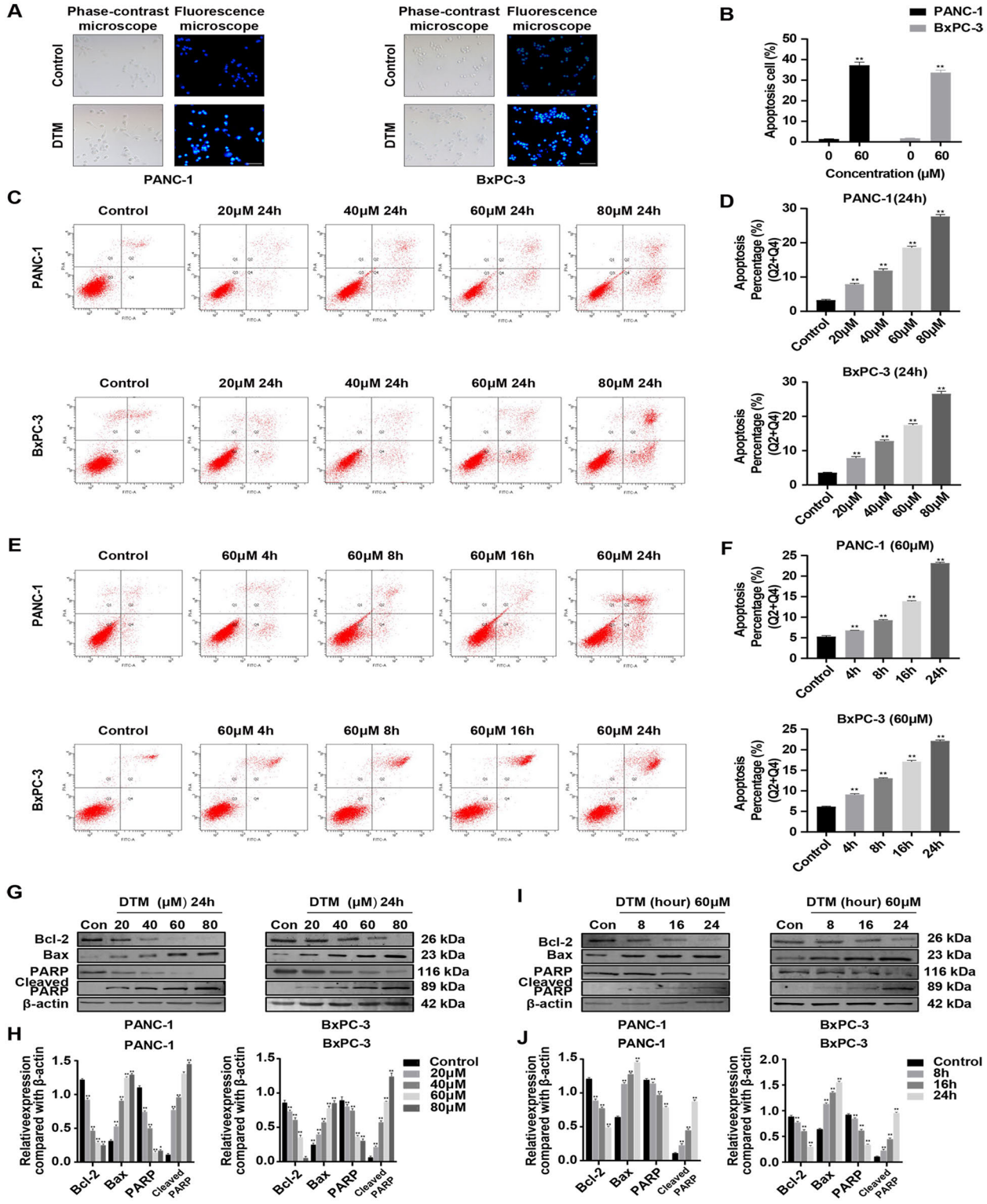

Figure 5. DTM induces apoptosis in PC cells. A) Morphological changes in apoptotic nuclei in the two groups were observed by performing Hoechst 33342 staining and viewing the cells under a fluorescence microscope (magnification: ×200; scale bar = 100 μm). B) The apoptotic cells in each group were quantitated. C, F) Apoptosis assays using the two PC cell lines treated with DTM (0–80 μM) for 24 h or with DTM (60 μM) for 0, 4, 8, 16, and 24 h. D, E) Quantification of apoptotic cells. G, I) Densitometric analysis of the expression of apoptosis-related proteins. H, J) Bar graphs represent relative protein expression. Notes: The analysis results are presented as the means ± standard deviations (n=3); *p<0.05, compared with the control group; **p<0.01, compared with the control group. Abbreviations: DTM-dictamnine; PC-pancreatic cancer

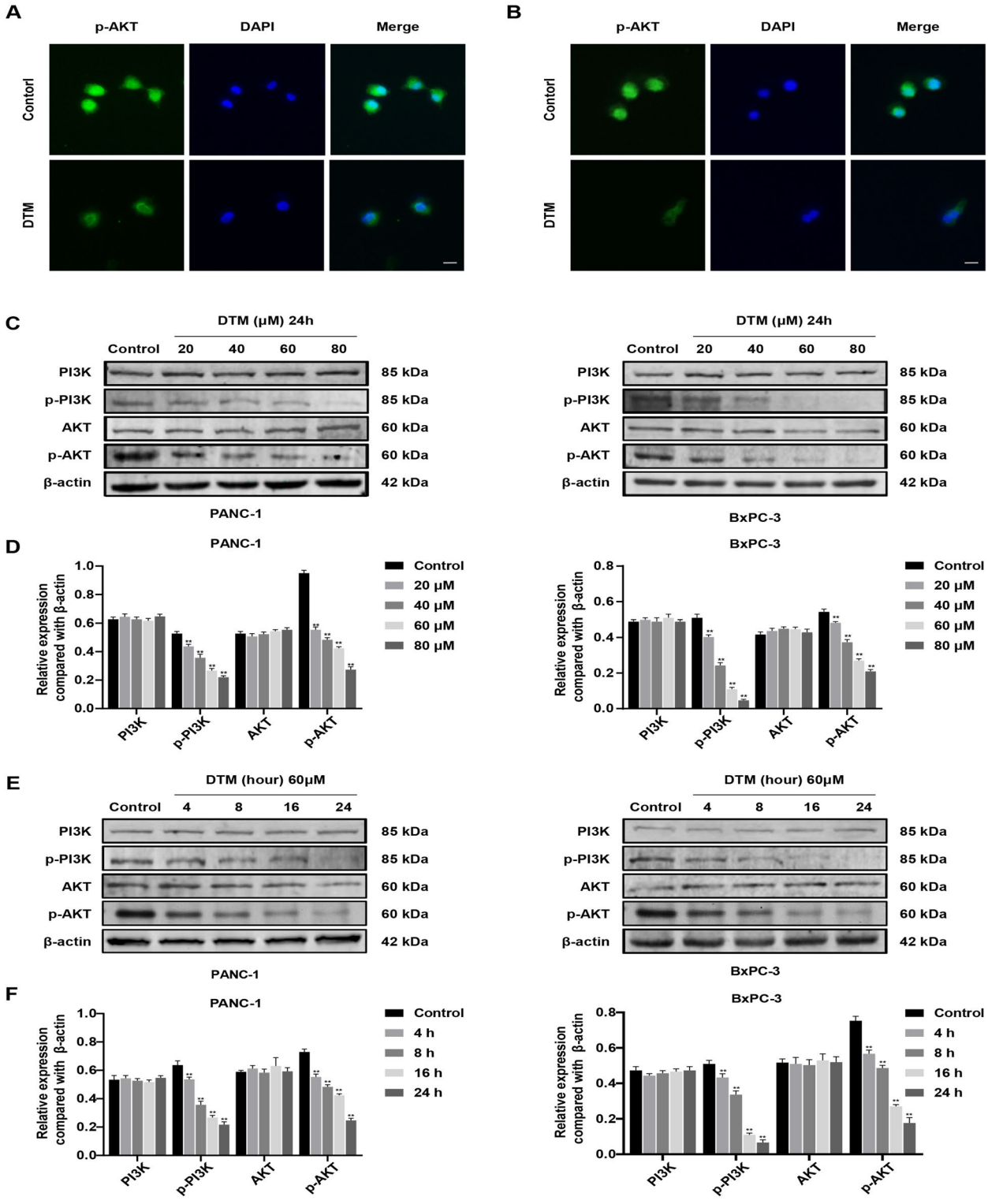

Figure 6. DTM inhibits PI3K/AKT phosphorylation and prevents the nuclear translocation of p-AKT. A, B) Representative images of cells detected by immunofluorescence staining with anti-p-AKT antibody after treatment with DTM (60 μM, 24 h) (magnification: ×200; scale bar = 10 μm). C, D) Western blots showing concentration- and time-dependent changes in the p-PI3K/p-AKT levels in DTM-treated PC cells. E, F) Bar graphs represent relative protein expression. Notes: The analysis results are presented as the means ± standard deviations (n=3); *p<0.05, compared with the control group; **p<0.01, compared with the control group. Abbreviations: DTM-dictamnine; PC-pancreatic cancer; PI3K-phosphatidylinositol-3 kinase; AKT-protein kinase B

in humans. In addition, several studies have indicated that excessive activation of the PI3K/AKT signaling occurs in approximately 50% of all PC cases and is usually related to an undifferentiated tumor state and an unfavorable patient prognosis [18, 22, 23]. Therefore, we postulated that DTM might affect PC development by regulating PI3K/AKT signaling and carried out subsequent experimental verification. Immunofluorescence assays indicated a markedly decreased level of nuclear p-AKT in PC cells treated with DTM (60 μM) for 24 h, and nuclear translocation of p-AKT was effectively prevented (Figures 6A, 6B). Moreover, western blotting results indicated concentration- and time-dependent decreases in the p-PI3K and p-AKT protein levels in cultured cells treated with DTM, but the total PI3K and AKT protein levels were unchanged (Figures 6C–6F). The above results indicate that DTM is an upstream inhibitor of p-AKT. Moreover, the influence of DTM on the malignant behavior of PC is most likely realized through the PI3K/AKT signaling pathway.

DTM docks at the binding site of PI3K and AKT. Because activation of the PI3K/AKT signaling pathway depends on either autophosphorylation or transphosphorylation by other molecules, to verify the correctness of the immunofluorescence results, we investigated whether the suppression of PI3K/AKT phosphorylation by DTM was due to direct binding. The theoretical binding mode of DTM with the key molecule AKT is described in Figure 7A. The interactions between DTM and the Lys143, Phe182, and Pro180 residues of AKT involve strong hydrogen bonds, with binding energies ranging from −3.19 to −4.85 kcal/mol, and this tight binding conformation of DTM to AKT directly changes the function of AKT. The theoretical combination of DTM and PI3K was also predicted, as shown in Figure 7B. DTM purportedly binds inside the hydrophobic pocket of PI3K with a compact conformation; the pocket is surrounded by Tyr867, Ile879, Val882, and Glu880 residues, which form hydrophobic bonds with DTM. These molecular docking results could explain the interactions between DTM and PI3K/AKT, particularly the DTM interaction with multiple amino acid residues in AKT via hydrogen bonding, which may prevent auto- or transphosphorylation through allosteric effects and ultimately lead to inactivation of the PI3K/AKT signaling pathway.

DTM suppresses tumor progression in a PC xenograft mouse model. Based on the results of the *in vitro* studies, we further evaluated the effect of DTM on tumorigenesis *in vivo* using a BxPC-3 cell xenograft tumor model. The tumor volume in mice intraperitoneally injected with DTM (15 mg/kg) was monitored for four weeks, and protein expression in tumor tissues was examined after the mice were euthanized. According to Figure 8A, the tumor volumes in the mice in the DTM-treated group were effectively reduced compared with those in the control group, and growth graphs illustrated a lower tumor growth rate in the DTM-treated group

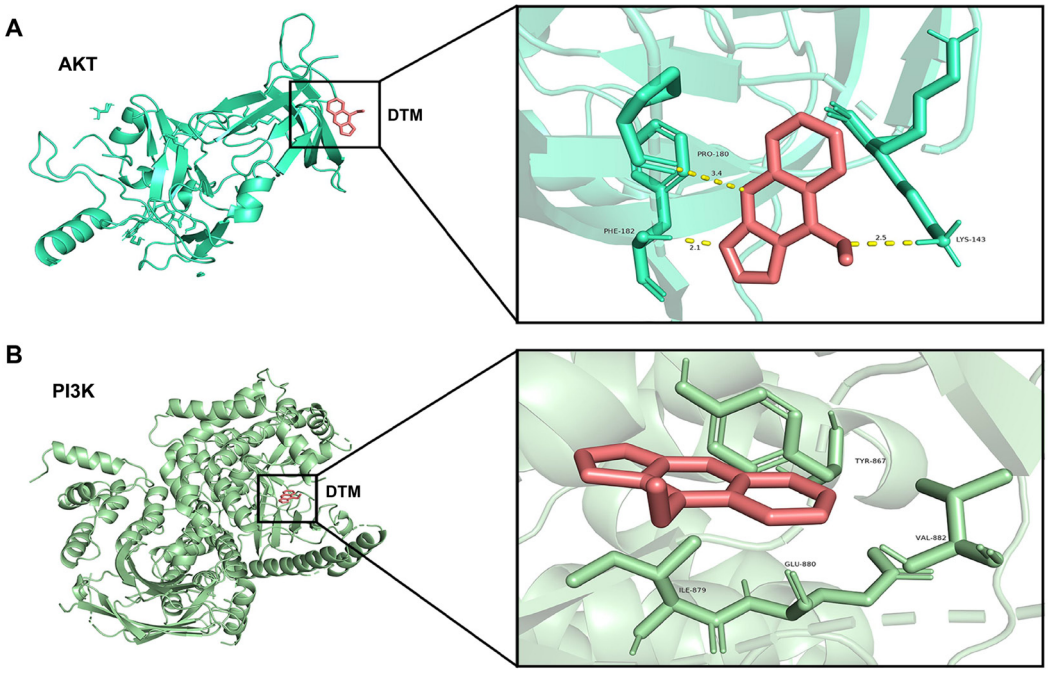

Figure 7. Molecular interactions of DTM with PI3K and AKT. A) Molecular docking of DTM with AKT. The hydrogen bond lengths of residues Phe182, Lys143, and Pro180 were 2.1, 2.5, and 3.4 angstroms, respectively. B) Molecular docking of DTM with PI3K. DTM is surrounded by residues Tyr867, Ile879, Val882, and Glu880 of PI3K, forming strong hydrophobic bonds. Notes: The analysis results are presented as the means ± standard deviations (n=3); *p<0.05, compared with the control group; **p<0.01, compared with the control group. Abbreviations: DTM-dictamnine; PI3K-phosphatidylinositol-3 kinase; AKT-protein kinase B

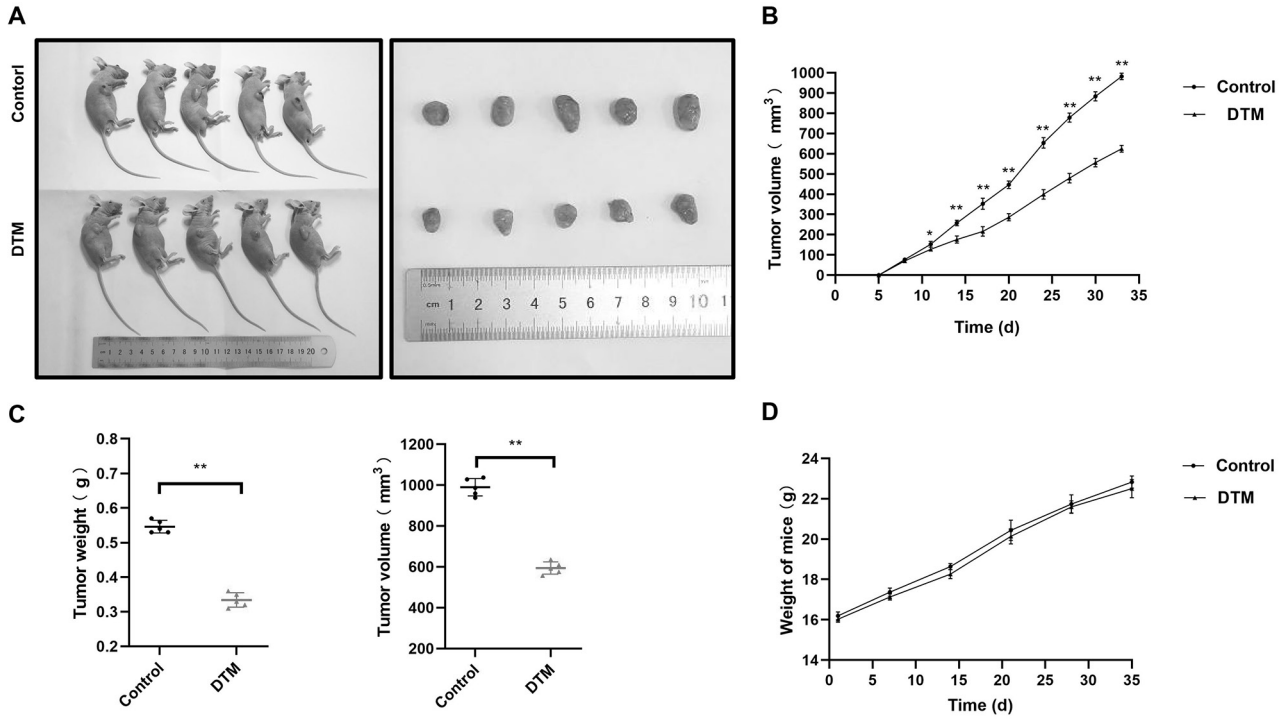

Figure 8. DTM suppresses tumor progression in PC xenograft mouse models. A) BXPC-3 cell xenografts were collected and photographed 35 days after transplantation. B) Growth curve for monitoring tumor volume. C) Tumor weights and volumes were calculated. D) The weight of mice was measured weekly. Notes: The analysis results are presented as the means ± standard deviations (n=3); *p<0.05, compared with the control group; **p<0.01, compared with the control group. Abbreviations: DTM-dictamnine; PC-pancreatic cancer

(Figure 8B). Based on the quantitative analysis results, we concluded that the tumors from mice in the control group were larger and exhibited a higher tumor volume than those from mice in the DTM-treated group (Figure 8C); however, the body weights of the mice in the two groups were nearly identical (Figure 8D).

Western blot analysis showed substantial decreases in vimentin, β-catenin, cyclin D1, CDK6, Bcl-2, and PARP levels in the tumor tissues from DTM-treated mice; in contrast, E-cadherin, P21, P27, Bax, and cleaved PARP levels showed an increasing trend *in vivo* (Figures 9A–9D). Meanwhile, p-PI3K and p-AKT levels were significantly decreased but total PI3K and AKT levels were unchanged in the tumor tissues (Figures 9E, 9F).

IHC staining was employed to assess the levels of progression-related markers in xenograft tumors from the two mouse groups. As illustrated in Figures 10A and 10B, Ki-67, p-PI3K, p-AKT, and CDK6 levels were decreased in the DTM-treated group compared with the control group, in contrast to the differences in cleaved PARP levels between the DTM-treated group and control group.

Histological evaluation of the liver and kidney via H&E staining revealed no distinct structural difference between the two groups (Figure 10C). We evaluated liver and kidney function based on standardized criteria to determine the potential toxicity of DTM, and no evident negative effects were observed in either treatment group (Figure 10D). In summary, all results showed that DTM effectively suppresses the growth of PC and has no apparent toxicity in mice. DTM also has specific cytotoxicity to cancer cells *in vivo*, and these results were consistent with those of our *in vitro* experiments.

Discussion

Despite the progress achieved in PC treatment, it remains one of the most lethal tumors worldwide, and less than 5% of patients survive more than 5 years. As the basic chemotherapy modality, gemcitabine shows a relatively low response rate (effectiveness < 12%) and leads to chemotherapy resistance to some extent [24–26]. Therefore, new therapeutic agents designed to prolong the survival of PC patients are highly desirable. In the present study, DTM exhibited antineoplastic effects by inducing cell cycle arrest, promoting apoptosis, and inhibiting migration and invasion ability in both PC cell lines. To explain the underlying mechanism by which DTM restrained tumor cell proliferation and EMT progression, we performed immunofluorescence, western blotting, and molecular docking studies (Figures 6, 7). Analysis of experimental results indicated that DTM plays an antitumor role by inhibiting the PI3K/AKT signaling pathway. Then,

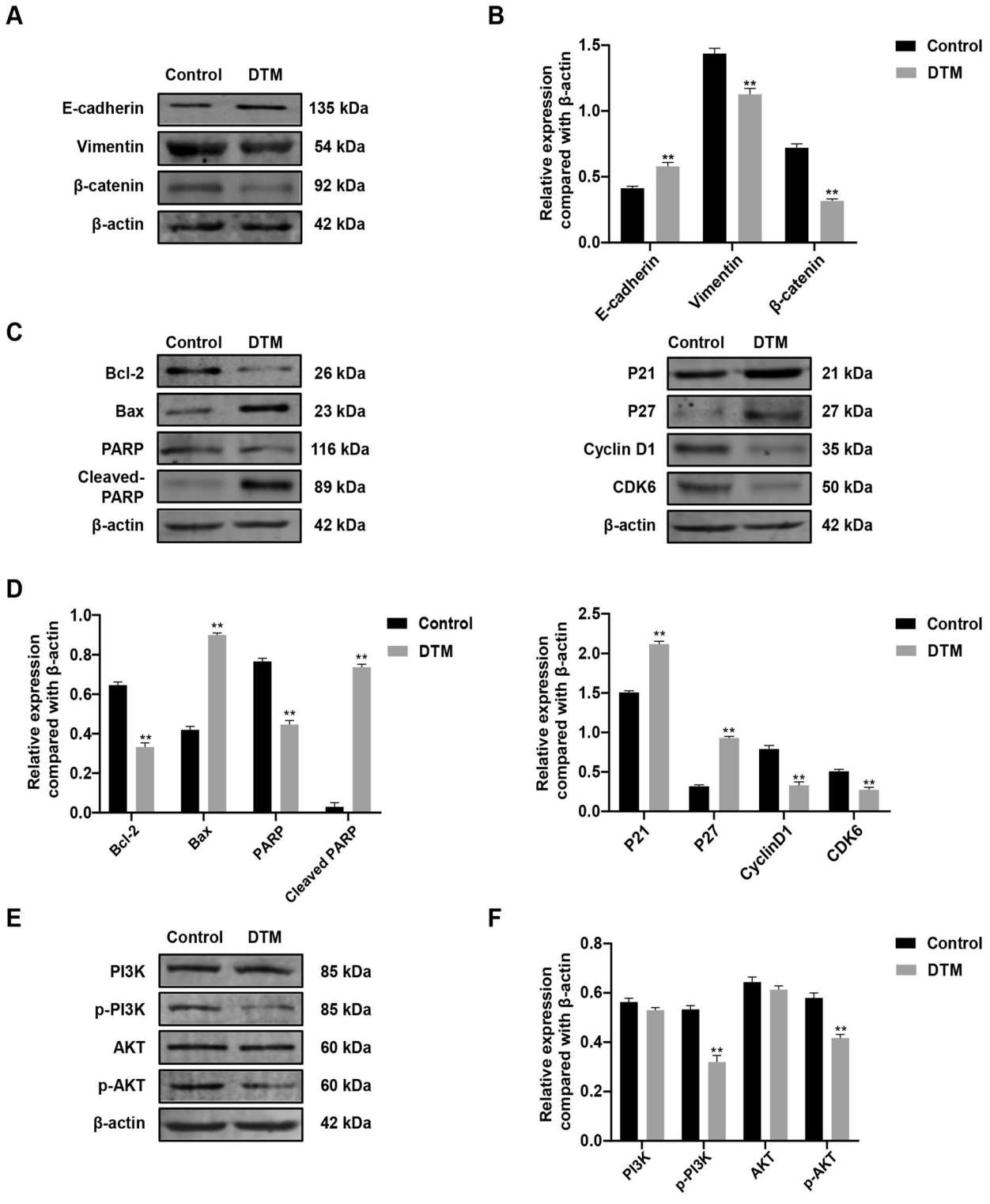

Figure 9. DTM alters the levels of proteins closely related to tumor progression *in vivo*. After completion of the treatment regimen, fresh tumor tissues excised from nude mice in the DTM-treated and control groups were processed, and protein levels were detected via western blotting. A, C, E) The levels of progression-related proteins were assessed in xenograft tumors using western blotting. B, D, F) Bar graphs represent progression-related protein levels. Notes: The analysis results are presented as the means ± standard deviations (n=3); *p<0.05, compared with the control group; **p<0.01, compared with the control group. Abbreviations: DTM-dictamnine

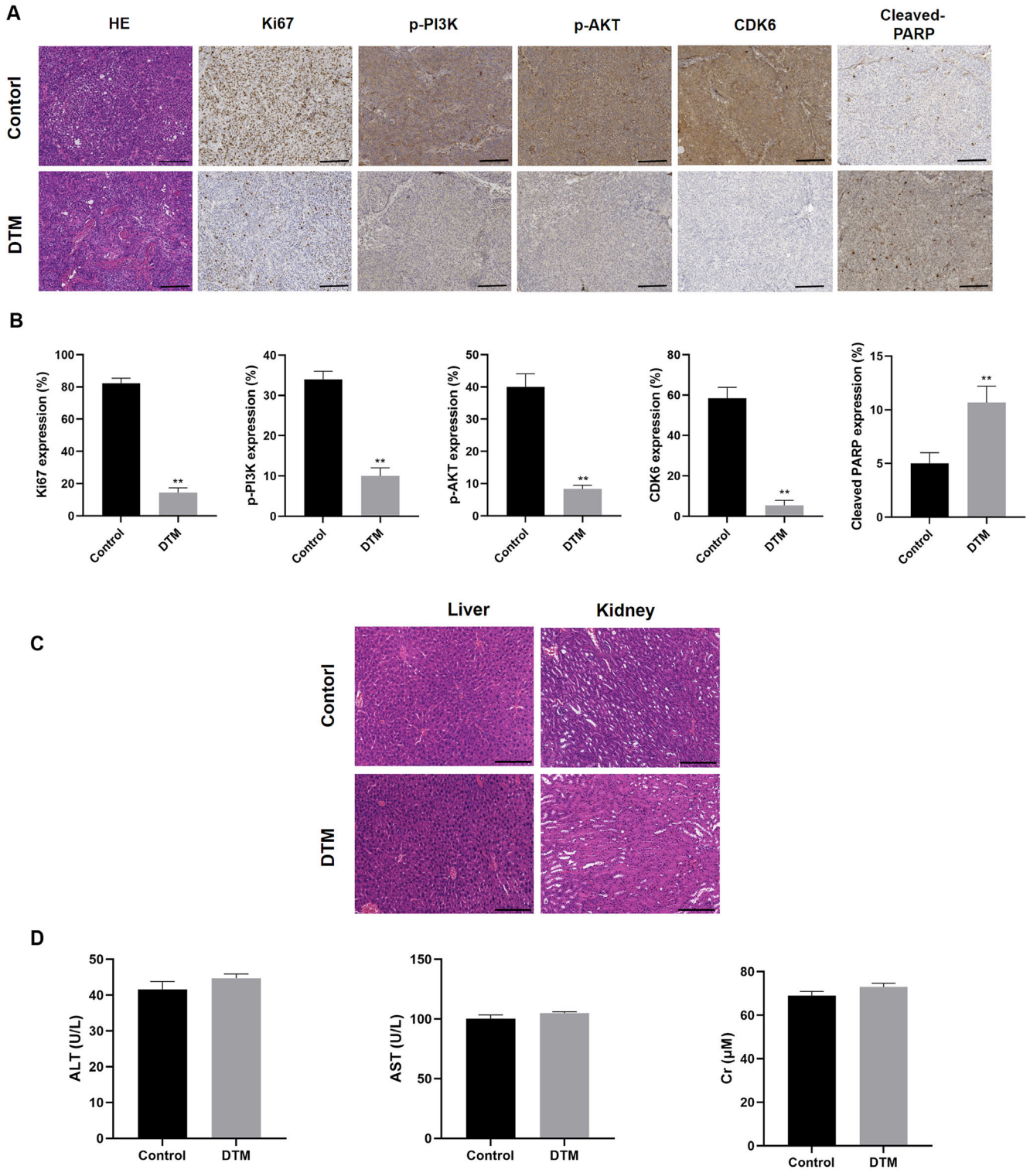

Figure 10. Related biological testing of tissue samples from model mice. A) The expression of Ki-67, p-PI3K, p-AKT, CDK6, and cleaved PARP in tumor tissues was measured using IHC staining. B) Quantitative analysis of IHC staining for the indicated proteins. C) H&E staining is presented to illustrate differences in liver and kidney histology between the two groups (magnification: ×100; scale bar = 200 μm). D) ALT, AST, and Cr levels in the blood of mice from each group were detected using ELISAs. Notes: The analysis results are presented as the means ± standard deviations (n=3); *p<0.05, compared with the control group; **p<0.01, compared with the control group.

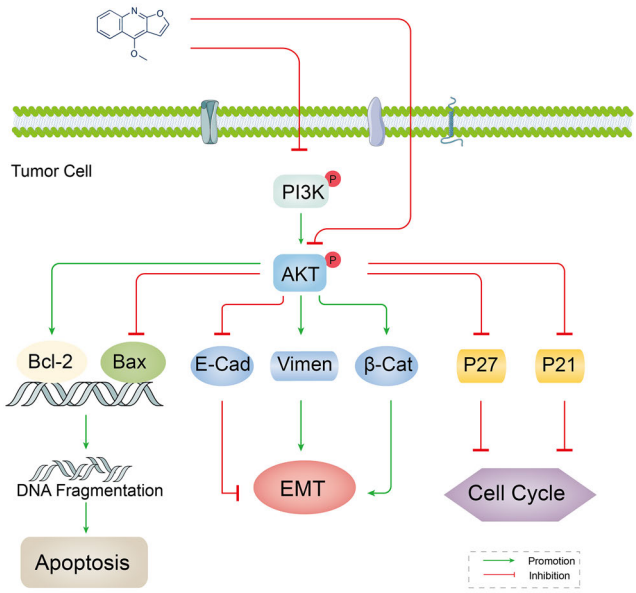

Figure 11. Schematic of the proposed mechanism by which DTM inhibits PC progression. DTM potentially blocks the PI3K/AKT signaling pathway to inhibit PC, but this effect requires further verification. Notes: The analysis results are presented as the means ± standard deviations (n=3); *p<0.05, compared with the control group; **p<0.01, compared with the control group. Abbreviations: DTM-dictamnine; PC-pancreatic cancer; PI3K-phosphatidylinositol-3 kinase; AKT-protein kinase B

the inactivation of the PI3K/AKT signaling pathway and the expression of downstream effectors after DTM treatment was confirmed.

First, we investigated the intrinsic molecular mechanism by which DTM induces PC cell cycle arrest (Figure 4). Cyclins and CDK complexes are crucial factors necessary for cell cycle completion, and binding of cyclin D1 to CDK6 activates transcription factors that promote the transcription of genes required for G1 to S phase progression and the initiation of cell proliferation [27, 28]. As a major step in cell proliferation, the successful transition of cells from the G1 to S phase is critical for cells to replicate all biomolecules related to cell division and ultimately complete mitosis. However, cyclin-CDK activities are controlled by cellular CDK inhibitors (CKIs). CKIs belong to the Cip/Kip family; mainly include $P27^{Kip1}$, $P21^{Cip1}$, and $P57^{KIP2}$; and are potent inhibitors of CDKs [29–31]. An overwhelming number of studies have reported that suppression of the PI3K/AKT signaling pathway can upregulate P27 and P21 expression and then downregulate cyclin D1 expression, inducing cell cycle arrest at the G0/G1 phase [32, 33]. Consistently, in our study, after DTM intervention, the expression of P21 and P27 was significantly increased, which directly led to a decrease in cyclin D1 and CDK6 levels, ultimately resulting in cell cycle arrest at the G0/G1 phase. Coincidentally, this trend is consistent with the changes observed in the main indicators of the PI3K/AKT signaling pathway. The results showed a possibility that the interaction between the PI3K/AKT signaling pathway and cyclin-CDK complexes is related to the blockade of cell cycle progression in PC.

Next, we revealed the potential mechanism by which DTM induces apoptosis in PC cells (Figure 5). Proteins in the Bcl-2 family are important for controlling apoptosis and mainly comprise anti-apoptotic proteins (e.g., Bcl-2 and Bcl-XL) and proapoptotic proteins (e.g., Bax and Bak). The interaction between members of the Bcl-2 family defines the boundary between pro- and anti-apoptotic activity [34]. Bax is a downstream effector of AKT, and inhibition of the p-AKT level contributes to a low Bcl-2/Bax ratio, which mediates the downstream activation of caspase proteins. Activated caspases cleave the pivotal death substrate PARP, decrease the mitochondrial membrane potential, and promote apoptosis of tumor cells [35–38]. In our study, we found that treatment with DTM increased Bax protein expression and reduced Bcl-2 protein expression, which led to a decreased Bcl-2/Bax ratio; these changes facilitated PARP cleavage and initiated PC cell apoptosis. DTM promoted PC cell apoptosis by adjusting the Bcl-2/Bax ratio via the PI3K/AKT signaling pathway, which may be the main mechanism by which DTM inhibits tumor proliferation.

In addition to its effects on cell cycle progression and apoptosis, DTM restrained PC cell migration and invasion through the PI3K/AKT signaling pathway (Figure 3). EMT is a complicated multistep process that plays an important role in promoting tumor invasion and metastasis. The most striking features of EMT are loss of E-cadherin expression and increased vimentin expression, which are considered critical processes in carcinoma progression [39]. In addition, proteins such as β-catenin are indispensable in this process [40]. Their joint actions lead to the continuous shifting of tumor cells towards an EMT phenotype. Although it has been reported that DTM regulates the expression of EMT-associated genes by downregulating HIF-α and slug, thereby reducing the migration and invasion abilities of carcinoma cells, plant-derived natural products reportedly inhibit tumor progression through different signaling pathways [8, 41]. The PI3K/AKT pathway is one of the most frequently altered signal transduction pathways in human cancer and has long been implicated in cancer metastasis through its ability to regulate the migration and invasion of tumor cells [13, 42]. As reported in the literature, inhibition of the PI3K/AKT signaling pathway can restrain PC cell migration and invasion *in vitro* by regulating EMT-related factors [14]. In DTM-treated PC cells, AKT activation was suppressed, preventing nuclear translocation of p-AKT; further regulating vimentin, β-catenin, and E-cadherin levels; and thus, restraining the EMT process. Therefore, the hypothesis that treatment with DTM inhibits EMT in PC cells by targeting the PI3K/AKT signaling pathway is reasonable and logical.

Multiple studies have focused on the development and innovative use of new drugs based on plant-derived natural products. Nevertheless, the problem of how to effectively

identify the proteins or genes targeted by these small molecules remains unsolved. Based on accumulating evidence, AKT is a major signaling molecule that regulates cell proliferation and growth, cell migration and invasion, glucose metabolism and angiogenesis, and approximately 50% of all human malignancies of various types exhibit alterations in the PI3K/AKT pathway [43, 44]. PI3K/AKT signaling is constitutively activated in the majority of PC patients and has been presented as a rational target for therapeutic intervention. PC growth is suppressed by inhibiting AKT activation [45, 46]. In our study, DTM inhibited AKT phosphorylation by either inactivating upstream PI3K or directly blocking its phosphorylation. Direct evidence of these possibilities was obtained via molecular docking analysis (Figure 7), which showed that DTM strongly interacts with PI3K and AKT by forming different chemical bonds that may directly lead to protein inactivation through allosteric effects. Excessive p-AKT levels were repressed due to DTM-mediated interference, and the nuclear translocation of activated AKT was hindered (Figure 6), thus affecting the activity of downstream effector proteins, such as P27, Bax, and E-cadherin, in PC cells (Figure 11) [47–50]. In addition, western blotting and immunohistochemical staining revealed a decreased level of p-AKT in the tumor tissues, consistent with the results of the *in vitro* experiments (Figures 9, 10A, and 10B). Moreover, toxicological experiments showed no apparent pathological changes in the visceral organs of DTM-treated animals (Figures 10C, 10D). All these findings indicate that DTM is an effective and safe potential drug for the treatment of PC.

Despite these notable findings, some limitations should be addressed. First, an *in vitro* test of AKT kinase activity in the presence or absence of DTM should provide conclusive evidence of the obvious effects of DTM on AKT. Second, the relationship between DTM restraint of PC cell proliferation and EMT remains to be further clarified. To remedy these design defects, we will perform more detailed experiments in the future.

In conclusion, DTM inhibits PC cell growth *in vitro* and *in vivo* while showing low hepatic and kidney toxicity. Furthermore, DTM restrains PC cell migration and invasion, induces apoptosis, and arrests cell cycle progression at G0/G1 phase; these effects are due to the inactivation of the PI3K/AKT signaling pathway. Our results provide evidence supporting the development of DTM as a promising therapeutic approach for PC treatment.

Supplementary information is available in the online version of the paper.

References

[1] LI D, XIE K, WOLFF R, ABBRUZZESE JL. Pancreatic cancer. Lancet 2004; 363: 1049–1057. https://doi.org/10.1016/S0140-6736(04)15841-8

[2] ILIC M, ILIC I. Epidemiology of pancreatic cancer. World J Gastroenterol 2016; 22: 9694–9705. https://doi.org/10.3748/wjg.v22.i44.9694

[3] MOORE A, DONAHUE T. Pancreatic Cancer. JAMA 2019; 322: 1426. https://doi.org/10.1001/jama.2019.14699

[4] WANG SJ, SUN B, CHENG ZX, ZHOU HX, GAO Y, et al. Dihydroartemisinininhibits angiogenesis in pancreatic cancer by targeting the NF-κB pathway. Cancer Chemother Pharmacol 2011; 68: 1421–1430. https://doi.org/10.1007/s00280-011-1643-7

[5] YANG GH, CHEN DF. Alkaloids from the roots of Zanthoxylum nitidum and their antiviral and antifungal effects. Chem Biodivers 2008; 5: 1718–1722. https://doi.org/10.1002/cbdv.200890160

[6] GAO X, ZHAO PH, HU JF. Chemical constituents of plants from the genus Dictamnus. Chem Biodivers 2011; 8: 1234–1244. https://doi.org/10.1002/cbdv.201000132

[7] SUN JB, QU W, GUAN FQ, LI LZ, LIANG JY. A new quinoline alkaloid from the roots of Dictamnus angustifolius. Chin J Nat Med 2014; 12: 222–224. https://doi.org/10.1016/S1875-5364(14)60037-6

[8] WANG JY, WANG Z, LI MY, ZHANG Z, MI C et al. Dictamnine promotes apoptosis and inhibits epithelial-mesenchymal transition, migration, invasion and proliferation by downregulating the HIF-1α and Slug signaling pathways. Chem Biol Interact 2018; 296: 134–144. https://doi.org/10.1016/j.cbi.2018.09.014

[9] GRILLE SJ, BELLACOSA A, UPSON J, KLEIN-SZANTO AJ, VAN ROY F et al. The protein kinase Akt induces epithelial mesenchymal transition and promotes enhanced motility and invasiveness of squamous cell carcinoma lines. Cancer Res 2003; 63: 2172–2178.

[10] VLEMINCKX K, VAKAET L JR, MAREEL M, FIERS W, VAN ROY F. Genetic manipulation of E-cadherin expression by epithelial tumor cells reveals an invasion suppressor role. Cell 1991; 66: 107–119. https://doi.org/10.1016/0092-8674(91)90143-m

[11] LIU QQ, CHEN K, YE Q, JIANG XH, SUN YW. Oridonin inhibits pancreatic cancer cell migration and epithelial-mesenchymal transition by suppressing Wnt/β-catenin signaling pathway. Cancer Cell Int 2016; 16: 57. https://doi.org/10.1186/s12935-016-0336-z

[12] SONG YX, XU ZC, LI HL, YANG PL, DU JK et al. Overexpression of GP73 promotes cell invasion, migration and metastasis by inducing epithelial-mesenchymal transition in pancreatic cancer. Pancreatology 2018; 18: 812–821. https://doi.org/10.1016/j.pan.2018.08.009

[13] LI W, JIANG ZD, XIAO X, WANG Z, WU Z et al. Curcumin inhibits superoxide dismutase-induced epithelial-to-mesenchymal transition via the PI3K/Akt/NF-κB pathway in pancreatic cancer cells. Int J Oncol 2018; 52: 1593–1602. https://doi.org/10.3892/ijo.2018.4295

[14] LI W, MA JG, MA QY, LI B, HAN L et al. Resveratrol inhibits the epithelial-mesenchymal transition of pancreatic cancer cells via suppression of the PI-3K/Akt/NF-κB pathway. Curr Med Chem 2013; 20: 4185–4194. https://doi.org/10.2174/09298673113209990251

[15] CANTLEY LC. The phosphoinositide 3-kinase pathway. Science 2002; 296: 1655–1657. https://doi.org/10.1126/science.296.5573.1655
[16] FRUMAN DA, CHIU H, HOPKINS BD, BAGRODIA S, CANTLEY LC et al. The PI3K Pathway in Human Disease. Cell 2017; 170: 605–635. https://doi.org/10.1016/j.cell.2017.07.029
[17] VIVANCO I, SAWYERS CL. The phosphatidylinositol 3-Kinase AKT pathway in human cancer. Nat Rev Cancer 2002; 2: 489–501. https://doi.org/10.1038/nrc839
[18] CHEN YW, BAI XL, ZHANG Q, WEN L, SU W et al. The hepatitis B virus X protein promotes pancreatic cancer through modulation of the PI3K/AKT signaling pathway. Cancer Lett 2016; 380: 98–105. https://doi.org/10.1016/j.canlet.2016.06.011
[19] BAO RF, SHU YJ, WU XS, WENG H, DING Q et al. Oridonin induces apoptosis and cell cycle arrest of gallbladder cancer cells via the mitochondrial pathway. BMC Cancer 2014; 14: 217. https://doi.org/10.1186/1471-2407-14-217
[20] BOHNACKER T, PROTA AE, BEAUFILS F, BURKE JE, MELONE A et al. Deconvolution of Buparlisib's mechanism of action defines specific PI3K and tubulin inhibitors for therapeutic intervention. Nat Commun 2017; 8: 14683. https://doi.org/10.1038/ncomms14683
[21] QUAMBUSCH L, LANDEL I, DEPTA L, WEISNER J, UHLENBROCK N et al. Covalent-Allosteric Inhibitors to Achieve Akt Isoform-Selectivity. Angew Chem Int Ed Engl 2019; 58: 18823–18829. https://doi.org/10.1002/anie.201909857
[22] SCHLIEMAN MG, FAHY BN, RAMSAMOOJ R, BECKETT L, BOLD RJ. Incidence, mechanism and prognostic value of activated AKT in pancreas cancer. Br J Cancer 2003; 89: 2110–2115. https://doi.org/10.1038/sj.bjc.6601396
[23] ESER S, REIFF N, MESSER M, SEIDLER B, GOTTSCHALK K et al. Selective requirement of PI3K/PDK1 signaling for Kras oncogene-driven pancreatic cell plasticity and cancer. Cancer Cell 2013; 23: 406–420. https://doi.org/10.1016/j.ccr.2013.01.023
[24] LONG J, ZHANG YQ, YU XJ, YANG JX, LEBRUN DG et al. Overcoming drug resistance in pancreatic cancer. Expert Opin Ther Targets 2011; 15: 817–828. https://doi.org/10.1517/14728222.2011.566216
[25] STATHIS A, MOORE MJ. Advanced pancreatic carcinoma: current treatment and future challenges. Nat Rev Clin Oncol 2010; 7: 163–172. https://doi.org/10.1038/nrclinonc.2009.236
[26] INAL A, KOS FT, ALGIN E, YILDIZ R, DIKILTAS M et al. Gemcitabine alone versus combination of gemcitabine and cisplatin for the treatment of patients with locally advanced and/or metastatic pancreatic carcinoma: a retrospective analysis of multicenter study. Neoplasma 2012; 59: 297–301. https://doi.org/10.4149/neo_2012_038
[27] GRAÑA X, REDDY EP. Cell cycle control in mammalian cells: role of cyclins, cyclin dependent kinases (CDKs), growth suppressor genes and cyclin-dependent kinase inhibitors (CKIs). Oncogene 1995; 11: 211–219.
[28] LUNDBERG AS, WEINBERG RA. Functional inactivation of the retinoblastoma protein requires sequential modification by at least two distinct cyclin-cdk complexes. Mol Cell Biol 1998; 18: 753–761. https://doi.org/10.1128/MCB.18.2.753
[29] NAKAYAMA K, NAKAYAMA K. Cip/Kip cyclin-dependent kinase inhibitors: brakes of the cell cycle engine during development. Bioessays 1998; 20: 1020–1029. https://doi.org/10.1002/(SICI)1521-1878(199812)20:12<1020::AID-BIES8>3.0.CO;2-D
[30] SHERR CJ. Cancer cell cycles. Science 1996; 274: 1672–1677. https://doi.org/10.1126/science.274.5293.1672
[31] REN S, XING YW. WANG CB, JIANG FQ, LIU GY et al. Fraxetin inhibits the growth of colon adenocarcinoma cells via the Janus kinase 2/signal transducer and activator of transcription 3 signalling pathway. Int J Biochem Cell Biol 2020; 125: 105777. https://doi.org/10.1016/j.biocel.2020.105777
[32] YANG WT, CHEN M, XU R, ZHENG PS. PRDM4 inhibits cell proliferation and tumorigenesis by inactivating the PI3K/AKT signaling pathway through targeting of PTEN in cervical carcinoma. Oncogene 2021; 40: 3318–3330. https://doi.org/10.1038/s41388-021-01765-x
[33] CLARKE RB. p27KIP1 phosphorylation by PKB/Akt leads to poor breast cancer prognosis. Breast Cancer Res 2003; 5: 162–163. https://doi.org/10.1186/bcr596
[34] YOULE RJ, STRASSER A. The BCL-2 protein family: opposing activities that mediate cell death. Nat Rev Mol Cell Biol 2008; 9: 47–59. https://doi.org/10.1038/nrm2308
[35] WANG HW, LI HL, CHEN FQ, LUO J, GU J et al. Baicalin extracted from Huangqin (Radix Scutellariae Baicalensis) induces apoptosis in gastric cancer cells by regulating B cell lymphoma (Bcl-2)/Bcl-2-associated X protein and activating caspase-3 and caspase-9. J Tradit Chin Med 2017; 37: 229–235. https://doi.org/10.1016/s0254-6272(17)30049-3
[36] SHAMAS-DIN A, KALE J, LEBER B, ANDREWS DW. Mechanisms of action of Bcl-2 family proteins. Cold Spring Harb Perspect Biol 2013; 5: a008714. https://doi.org/10.1101/cshperspect.a008714
[37] PAL S, PAL PB, DAS J, SIL PC. Involvement of both intrinsic and extrinsic pathways in hepatoprotection of arjunolic acid against cadmium induced acute damage in vitro. Toxicology 2011; 283: 129–139. https://doi.org/10.1016/j.tox.2011.03.006
[38] XIN MG, DENG XM. Nicotine inactivation of the proapoptotic function of Bax through phosphorylation. J Biol Chem 2005; 280: 10781–10789. https://doi.org/10.1074/jbc.M500084200
[39] MARIE-EGYPTIENNE DT, LOHSE I, HILL RP. Cancer stem cells, the epithelial to mesenchymal transition (EMT) and radioresistance: potential role of hypoxia. Cancer Lett 2013; 341: 63–72. https://doi.org/10.1016/j.canlet.2012.11.019
[40] KALLURI R, WEINBERG RA. The basics of epithelial-mesenchymal transition. J Clin Invest 2009; 119: 1420–1428. https://doi.org/10.1172/JCI39104
[41] DONG BZ, YANG ZJ, JU Q, ZHU SG, WANG YX et al. Anticancer Effects of Fufang Yiliu Yin Formula on Colorectal Cancer Through Modulation of the PI3K/Akt Pathway and BCL-2 Family Proteins. Front Cell Dev Biol 2020; 8: 704. https://doi.org/10.3389/fcell.2020.00704

[42] ZHANG Y, JIN F, LI XC, SHEN FJ, MA XL et al. The YY1-HOTAIR-MMP2 Signaling Axis Controls Trophoblast Invasion at the Maternal-Fetal Interface. Mol Ther 2017; 25: 2394–2403. https://doi.org/10.1016/j.ymthe.2017.06.028

[43] BURRIS HA 3RD. Overcoming acquired resistance to anticancer therapy: focus on the PI3K/AKT/mTOR pathway. Cancer Chemother Pharmacol 2013; 71: 829–842. https://doi.org/10.1007/s00280-012-2043-3

[44] KOUNDOUROS N, POULAGAINNIS G. Phosphoinositide 3-Kinase/Akt Signaling and Redox Metabolism in Cancer. Front Oncol 2018; 8: 160. https://doi.org/10.3389/fonc.2018.00160

[45] BONDAR VM, SWEENEY-GOTSCH B, ANDREEFF M, MILLS GB, MCCONKEY DJ. Inhibition of the phosphatidylinositol 3'-kinase-AKT pathway induces apoptosis in pancreatic carcinoma cells in vitro and in vivo. Mol Cancer Ther 2002; 1: 989–997. https://doi.org/10.3389/fonc.2018.00160

[46] WEI WT, CHEN H, WANG ZH, NI ZL, LIU HB et al. Enhanced antitumor efficacy of gemcitabine by evodiamine on pancreatic cancer via regulating PI3K/Akt pathway. Int J Biol Sci 2012; 8: 1–14. https://doi.org/10.7150/ijbs.8.1

[47] MANNING BD, CANTLEY LC. AKT/PKB signaling: navigating downstream. Cell 2007; 129: 1261–1274. https://doi.org/10.1016/j.cell.2007.06.009

[48] MANNING BD, TOKER A. AKT/PKB Signaling: Navigating the Network. Cell 2017; 169: 381–405. https://doi.org/10.1016/j.cell.2017.04.001

[49] ZHU JH, DE MELLO RA, YAN QL, WANG JW, CHEN Y et al. MiR-139-5p/SLC7A11 inhibits the proliferation, invasion and metastasis of pancreatic carcinoma via PI3K/Akt signaling pathway. Biochim Biophys Acta Mol Basis Dis 2020; 1866: 165747. https://doi.org/10.1016/j.bbadis.2020.165747

[50] SONG SZ, LIN S, LIU JN, ZHANG MB, DU YT et al. Targeting of SPP1 by microRNA-340 inhibits gastric cancer cell epithelial-mesenchymal transition through inhibition of the PI3K/AKT signaling pathway. J Cell Physiol 2019; 234: 18587–18601. https://doi.org/10.1002/jcp.28497

https://doi.org/10.4149/neo_2022_211016N1474

Dictamnine inhibits pancreatic cancer cell growth and epithelial-mesenchymal transition by blocking the PI3K/AKT signaling pathway

Zhi-Qiang ZHANG[1], Wen-Liang XUAN[1], Yang HUANG[1], Shuo REN[2], Tu-Ya WULAN[1], Ye SONG[1], Dong-Bo XUE[1], Wei-Hui ZHANG[1,*]

Supplementary Information

Control

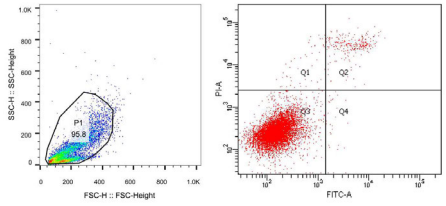

Tube: 1

Population	#Events	%Parent	%Total
All Events	23,861	####	100.0
P1	9,491	39.8	39.8
Q1	48	0.5	0.2
Q2	271	2.9	1.1
Q3	9,143	96.3	38.3
Q4	29	0.3	0.1

20μM 24h

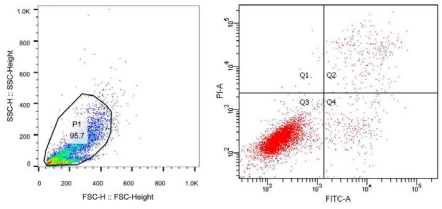

Tube: 2

Population	#Events	%Parent	%Total
All Events	7,962	####	100.0
P1	6,303	79.3	79.3
Q1	13	0.2	0.2
Q2	265	4.2	3.3
Q3	5,770	91.5	72.6
Q4	255	4.0	3.2

40μM 24h

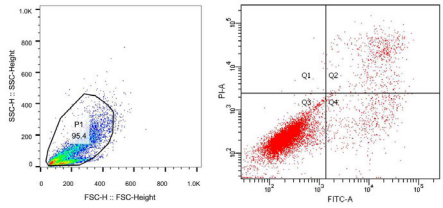

Tube: 3

Population	#Events	%Parent	%Total
All Events	13,333	####	100.0
P1	9,858	73.9	73.9
Q1	11	0.1	0.1
Q2	557	5.7	4.2
Q3	8,756	88.8	65.7
Q4	534	5.4	4.0

60μM 24h

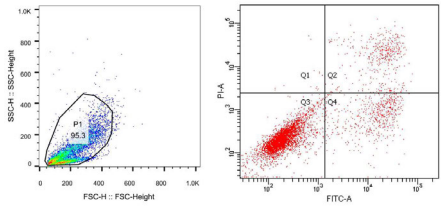

Tube: 4

Population	#Events	%Parent	%Total
All Events	8,513	####	100.0
P1	5,243	61.6	61.6
Q1	14	0.3	0.2
Q2	427	8.1	5.0
Q3	4,245	81.0	49.9
Q4	557	10.6	6.5

80μM 24h

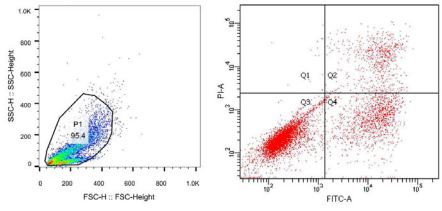

Tube: 5

Population	#Events	%Parent	%Total
All Events	12,163	####	100.0
P1	6,982	57.4	57.4
Q1	15	0.2	0.1
Q2	661	9.5	5.4
Q3	5,072	72.6	41.7
Q4	1,234	17.7	10.1

Supplementary Figure S1

Control

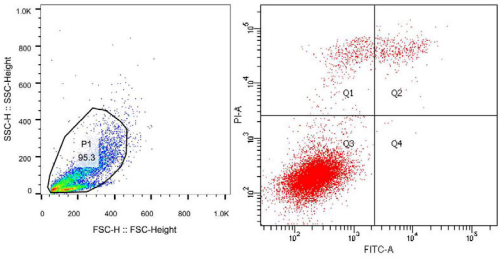

Tube: 1

Population	#Events	%Parent	%Total
All Events	10,303	####	100.0
P1	9,993	97.0	97.0
Q1	387	3.9	3.8
Q2	362	3.6	3.5
Q3	9,238	92.4	89.7
Q4	6	0.1	0.1

20μM 24h

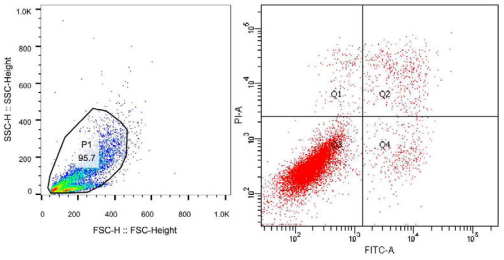

Tube: 2

Population	#Events	%Parent	%Total
All Events	11,940	####	100.0
P1	10,214	85.5	85.5
Q1	152	1.5	1.3
Q2	464	4.5	3.9
Q3	9,248	90.5	77.5
Q4	350	3.4	2.9

40μM 24h

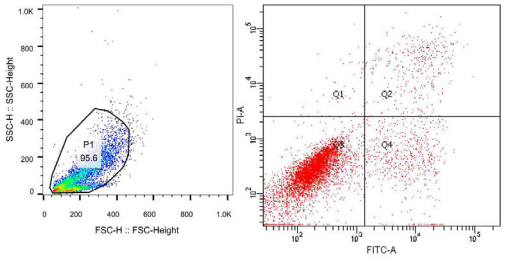

Tube: 3

Population	#Events	%Parent	%Total
All Events	29,507	####	100.0
P1	7,334	24.9	24.9
Q1	44	0.6	0.1
Q2	362	4.9	1.2
Q3	6,360	86.7	21.6
Q4	568	7.7	1.9

60μM 24h

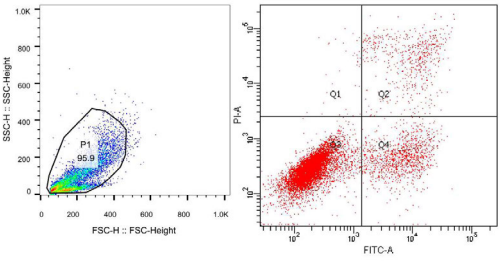

Tube: 4

Population	#Events	%Parent	%Total
All Events	11,512	####	100.0
P1	9,872	85.8	85.8
Q1	35	0.4	0.3
Q2	563	5.7	4.9
Q3	8,163	82.7	70.9
Q4	1,111	11.3	9.7

80μM 24h

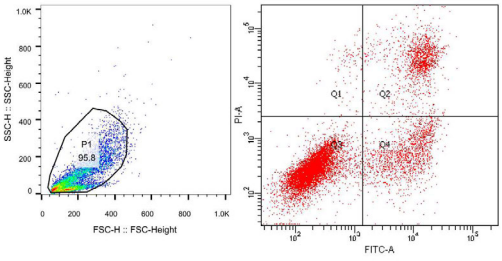

Tube: 5

Population	#Events	%Parent	%Total
All Events	16,121	####	100.0
P1	11,129	69.0	69.0
Q1	100	0.9	0.6
Q2	1,448	13.0	9.0
Q3	8,065	72.5	50.0
Q4	1,516	13.6	9.4

Supplementary Figure S2

Control

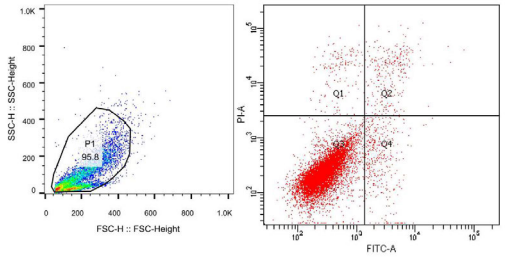

Tube: 1			
Population	#Events	%Parent	%Total
All Events	10,382	####	100.0
P1	10,045	96.8	96.8
Q1	153	1.5	1.5
Q2	278	2.8	2.7
Q3	9,225	91.8	88.9
Q4	389	3.9	3.7

60μM 4h

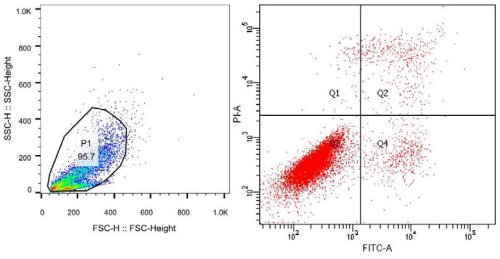

Tube: 2			
Population	#Events	%Parent	%Total
All Events	11,640	####	100.0
P1	10,173	87.4	87.4
Q1	83	0.8	0.7
Q2	426	4.2	3.7
Q3	9,186	90.3	78.9
Q4	478	4.7	4.1

60μM 16h

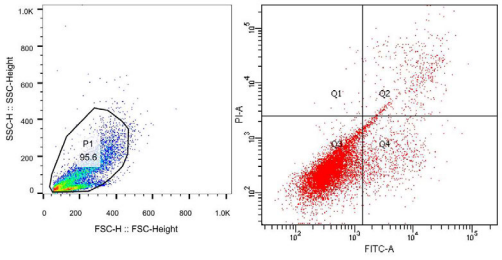

Tube: 4			
Population	#Events	%Parent	%Total
All Events	10,611	####	100.0
P1	10,081	95.0	95.0
Q1	19	0.2	0.2
Q2	479	4.8	4.5
Q3	8,691	86.2	81.9
Q4	892	8.8	8.4

60μM 8h

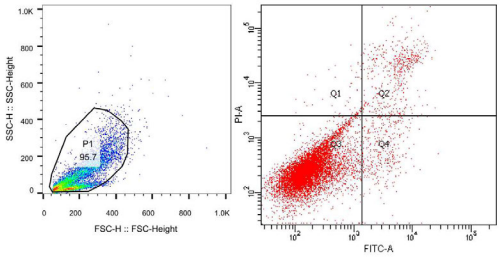

Tube: 3			
Population	#Events	%Parent	%Total
All Events	10,772	####	100.0
P1	10,106	93.8	93.8
Q1	66	0.7	0.6
Q2	530	5.2	4.9
Q3	9,118	90.2	84.6
Q4	392	3.9	3.6

60μM 24h

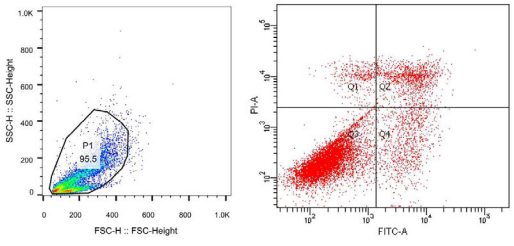

Tube: 5			
Population	#Events	%Parent	%Total
All Events	13,464	####	100.0
P1	10,050	74.6	74.6
Q1	385	3.8	2.9
Q2	1,222	12.2	9.1
Q3	7,433	74.0	55.2
Q4	1,010	10.0	7.5

Supplementary Figure S3

Control

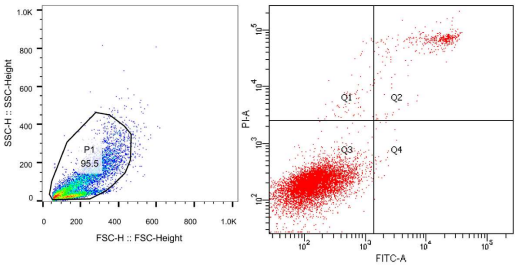

Tube: 1

Population	#Events	%Parent	%Total
All Events	21,462	####	100.0
P1	7,734	36.0	36.0
Q1	66	0.9	0.3
Q2	406	5.2	1.9
Q3	7,234	93.5	33.7
Q4	28	0.4	0.1

60μM 4h

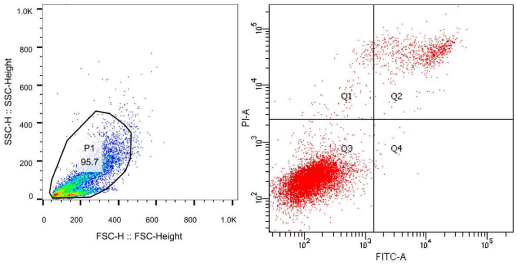

Tube: 2

Population	#Events	%Parent	%Total
All Events	10,246	####	100.0
P1	9,973	97.3	97.3
Q1	134	1.3	1.3
Q2	779	7.8	7.6
Q3	9,038	90.6	88.2
Q4	22	0.2	0.2

60μM 8h

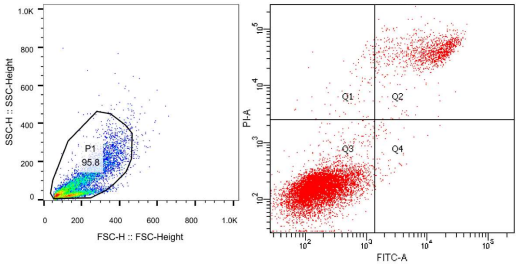

Tube: 3

Population	#Events	%Parent	%Total
All Events	10,553	####	100.0
P1	9,970	94.5	94.5
Q1	87	0.9	0.8
Q2	1,220	12.2	11.6
Q3	8,597	86.2	81.5
Q4	66	0.7	0.6

60μM 16h

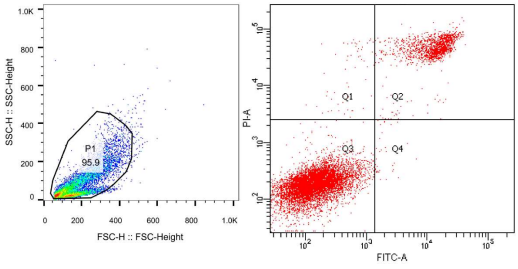

Tube: 4

Population	#Events	%Parent	%Total
All Events	10,744	####	100.0
P1	10,096	94.0	94.0
Q1	57	0.6	0.5
Q2	1,648	16.3	15.3
Q3	8,347	82.7	77.7
Q4	44	0.4	0.4

60μM 24h

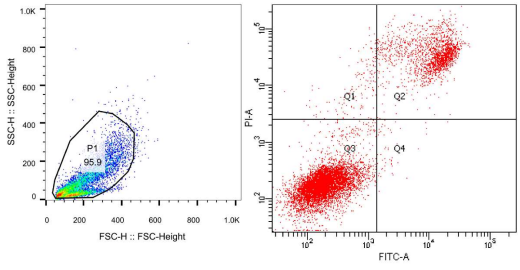

Tube: 5

Population	#Events	%Parent	%Total
All Events	10,951	####	100.0
P1	9,912	90.5	90.5
Q1	139	1.4	1.3
Q2	1,928	19.5	17.6
Q3	7,785	78.5	71.1
Q4	60	0.6	0.5

Supplementary Figure S4